Characterization of THz radiation by collimated wavefront aperture raster scanning

Daniel Nuño[(1)], María C. Santos[(1)], Juan S. Gómez-Díaz[(2)], Jordi Romeu[(1)] and Lluís Jofre[(1)]
E-mail santos@tsc.upc.edu.
(1) Dept. of Signal Theory and Communications, Universitat Politècnica de Catalunya, UPC-BarcelonaTECH
(2) Dept. of Electrical and Computer Engineering, University of California at Davis.

***Abstract*- We present measurements for characterization of the beam profile and polarization pattern of lens-coupled photoconductive antennas (PCAs) at THz frequencies using a setup with antennas at fixed positions and a movable aperture placed in between collimating THz lenses. The measured beam patterns for co-polar and cross-polar components reveal the expected Airy disc and quadrupole behavior, respectively. The temporal evolution of the polarization in the directions of maximum cross-polar component follows a single-cycle circle with opposite handedness at each side of the antennas line-of-sight (LOS). Results are consistent with those obtained with fiber-coupled movable antennas, while enjoying the simplicity of a free-space laser-PCA feed which does not require painstaking laser realignment for each beam direction measure.**

I. INTRODUCTION

Mastering the Terahertz domain of electromagnetic radiation has been one the most sought-after challenges of science and technology in recent times. Sandwiched in between the microwave and the infrared ranges of the spectrum, the once elusive Terahertz gap of the electromagnetic spectrum, ranging from 0.1 to 10 THz, has now been bridged, as efficient means of generation, detection and control of waves in this frequency range are becoming available in compact form and at a reasonable cost [1]. Terahertz spectroscopy systems are key to applications for non-destructive testing (NDT) in many areas of industry; for pieces and paint coating inspection, in automotive and aviation production lines [2]; for substances identification, in pharmaceutical and food industries [3]; for artwork inspection and conservation [4]; security imaging and screening and detection of concealed threats [5], and for clinical testing and early diagnosis and treatment [6], to name just a few of the most important. Even if it is true that the reduced propagation range, usually of only several cm, and severe degrading effect of atmospheric loss is presently hindering its progress in telecommunications, it is also expected that the promise of a vast unused spectrum will spur research efforts in a bandwidth-starving market [7].

In contrast to profuse attention devoted to the optimization of the temporal and spectral characteristics, the specifics of THz wave propagation and the spatial patterns have scarcely been explored [8]-[14], and also not many too detailed discussions of the features of wave polarization have been available [15]-[18]. On the other hand, even when fiber-coupled transceivers are customary in the market, fiber guiding of ultrashort laser pulses comes with a price in the form of a number of strenuous technological challenges [13,17]. Specifically, for comparative studies and characterization of the performance and influence of the various components and characteristics of a PCA system, such as for example the antenna geometry or the substrate coupling lens, a fiber connection can significantly increase both complexity and the system's adjustments and maintenance. A free-space laser-PCA feed is interesting to be able to easily replace the PCA or other elements of the setup for comparative performance studies. The characterization of the spatial beam and polarization patterns with fixed position THz antennas is thus found of interest.

In this paper we present results of our measurements on the characterization of the radiation pattern and polarization of THz PCA systems using a setup with fixed position antennas. This is relevant to time-domain spectrometers with a free-space ultrashort pulse coupling.

II. SETUP

Figure 1 shows the schematic of the laboratory setup used in measurements. Frequency-doubled femtosecond pulses at $\lambda = 780\ nm$ coming from a mode-locked Fiber laser and traveling through free-space, are split towards transmitter (TX) and receiver (RX) PCAs imprinted over low temperature grown Gallium Arsenide (LT-GaAs) substrates. A mechanical stage provides the relative delay between the laser pulses at the TX and RX antennas required for temporal sampling of the received signal, which is detected with maximum Signal to Noise Ratio (SNR) levels of 70 dB owing to lock-in amplification enabled by 10 kHz and 20 V amplitude square-wave modulation of the voltage bias of the TX PCA, with a 30 ms integration time base.

As probe antennas we have used silicon lens-coupled TX 60^0 flare angle bow-tie and RX H-dipole structures, with respective lengths $180\mu m$ and $20\mu m$. See dimensions and geometries in Figure 2. Average optical power levels of 10 mW are focused into the $10\ \mu m\ x\ 5\ \mu m$ antennas gap area. The aplanatic hyper-hemispherical substrate silicon lens that avoids back reflections at the substrate face due to critical angle incidence from high dielectric constant LT-AsGa has 12 mm diameter. The substrate lens-PCA alignment is adjusted manually through precision micromechanical positioners. It has been previously observed that displacements as small as 100 μm from the lens axis may cause a critical reduction of the coupling efficiency [10]. From our experience, even below

those values of displacement, the beam patterns may be altered quite significantly.

For wavefront collimation and focusing into the RX, two plano-convex lenses with diameter $D = 38\,mm$ and focal length $L = 5\,cm$ are placed perpendicular to the THz path, with symmetrical orientation, at one focal length distance from PCAs, see Figure 1. The lenses are separated by 10 cm, and a blocking screen made of 1 mm thick copper, with a 2 cm diameter aluminum iris that controls the size of a circular aperture, lays in between them, aligned to the plane perpendicular to the THz propagation, i. e. the *xy* plane in Figure 1. For automated beam pattern measure, the aperture may be scanned along the *x* and *y* directions through a 2D stepper controlled electronically.

The TX antenna is oriented with horizontal E-plane as in Figure 2. For assessment of the cross-polar polarization pattern, the RX antenna is rotated by 90º.

When analyzing the data, it is important to bear in mind that, under the approximations outlined in the following sections, the spatial profiles obtained using the proposed measurement setup will correspond to the product of the aperture-sampled beam patterns of both emitter and received antennas, at the targeted angular direction, sampled by the aperture location in the transverse *xy* plane.

The maximum excursion and step of the mechanical delay time sampling unit are selected to provide a maximum measurement bandwidth of 5 THz and 12.5 GHz frequency resolution. The measured total spectral bandwidth is thus limited by material parameters and the dispersive features of the elements in the experimental setup.

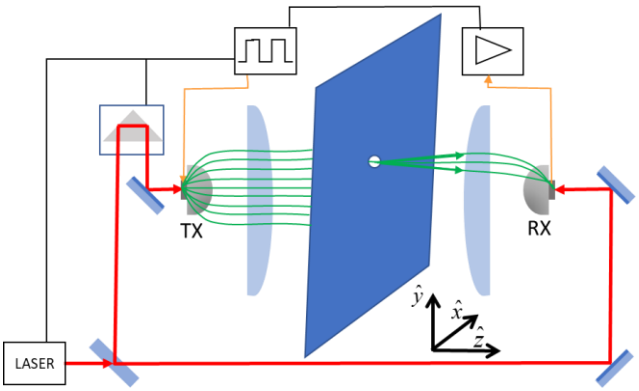

Fig. 1. Schematic drawing of the THz-TDS setup used for beam imaging experiments with fixed position antennas.

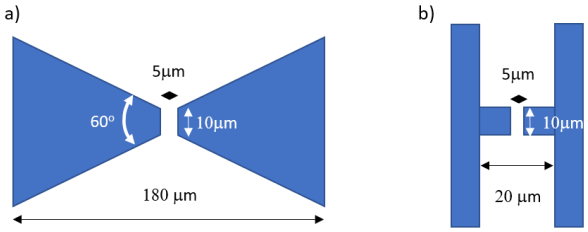

Fig. 2. Probe photoconductive antennas geometry and dimensions, a) TX, bow-tie, b) RX, H-dipole.

A. *Aperture dimensioning*

In this section we explore the effect of the aperture size. A trade off exists between spatial resolution of the sampled THz beam and collection efficiency of the pulse power. A good contrast for the power measurement requires SNR levels above a quality threshold. Looking in Fig. 3 at the power spectra measured for different aperture sizes with center at the antennas LOS axis ($x = y = 0$), an aperture size $a = 4\,mm$ is a sensible choice, yielding a maximum 70 dB SNR around 0.3 THz.

Diffractive effects are also expected to play a role because due to aperture diffraction, the wave arriving to the RX plano-convex lens may significantly deviate from a perfect collimated beam, limiting the lens focusing action. Considering a circular aperture, 84% of incident energy falls within the Airy disk [20], i.e. the first diffraction minimum. The diffractive cone out from the aperture will have an opening angle θ which can be estimated from

$$sin(\theta) \sim \frac{\lambda}{a} \qquad (1)$$

with λ the wavelength of the radiation. For our aperture choice and a minimum frequency of interest $f_{min} = 0.2\,THz$, the beam will feature a maximum aperture cone angle $\theta_{max} \sim 22^0$ which is taken as a safety limit to neglect diffractive effects in the beam pattern measure. A rigorous analysis of diffraction is left for future works. In view of the result, to ensure that the wave energy is fully collected inside the $D = 38\,mm$ diameter lens located at $l = 5\,cm$ from the aperture, we restrict transverse plane scans from -15 to $+15\,mm$.

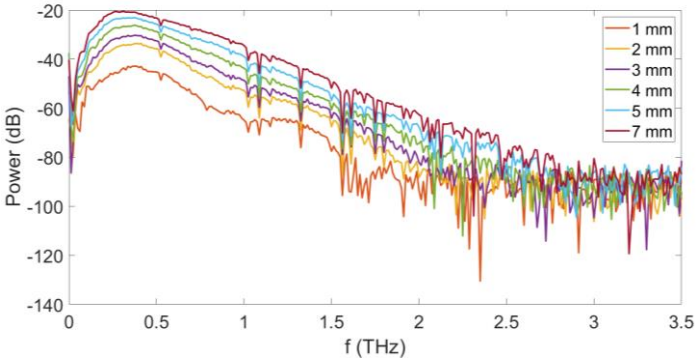

Fig. 3. Spectrum for different circular aperture diameters with aperture in the center of the scan area, *x=y=0*.

III. Results

Figure 4 shows measured beam patterns in both co-polar and cross-polar polarization components at selected frequencies. The Airy pattern feature that characterizes the THz radiation coupled to air through hyper-hemispherical silicon substrate lenses is clearly apparent in the co-polar component especially at the lower frequencies [10,12], while the cross-polar component follows the quadrupole behavior expected from the results and analysis in [15,16]. The observed beam patterns and their symmetry against LOS is indicative of a correct adjustment of the elements of the measuring system and thus it validates the measurement technique. The dependence with the lateral displacement seen in the three figures is consistent with the projection over the measurement plane of the angular dependence of the bow-tie and H-dipole silicon-lensed antennas.

In line with the measures with fiber-coupled antennas in [14], the patterns obtained lose definition as the frequency increases, due to the inherent power averaging of a fixed diameter aperture. The first diffraction nulls are clearly seen in the pattern at 0.25 THz at an angle $\theta_{null} \sim 8^0$, consistent with an effective radius of the substrate lens of 9 mm, a reasonable value for the nominal 12 mm, taking into account the Gauss-

Laguerre mode analysis for THz radiation of hyper-hemispherical lens-coupled PCAs in [13]. The cross-polar polarization maxima have been found at $\theta_{xmax}\sim 5{,}7^0$, in agreement with the findings in [16].

The beam pattern results in the temporal domain are summarized in the 2D color plots of Figure 5. As already noted in [15,16], the cross-polar component of both dipole and bow-tie antenna geometries features a null along the antennas LOS axis, and about 180º phase difference between the temporal waveforms at negative and positive x points at the same distance from LOS. A small angle tilt towards the positive x side is observed in the temporal patterns (indicated by a red dashed line in Figure 5 b), confirmed by a best fit of temporal waveforms taken at symmetrical points around LOS for a relative delay of the positive side of $\delta\tau = 0.07\ ps$ for each mm of distance from LOS. The angle tilt value is found as $\delta\theta\sim asin\left(c\frac{\delta\tau}{2mm}\right)\sim 0.6º$ with c the wave velocity in vacuum. This reveals the potential of spatial beam characterization, and especially of detection of the cross-polar component, for assessment of the quality of the measurement system, and for correction of even very small alignment errors. The availability of techniques to ensure the repeatability of measurements acquires special relevance when targeting the comparison of different designs of PCAs, as the system needs to be realigned every time the PCA is changed.

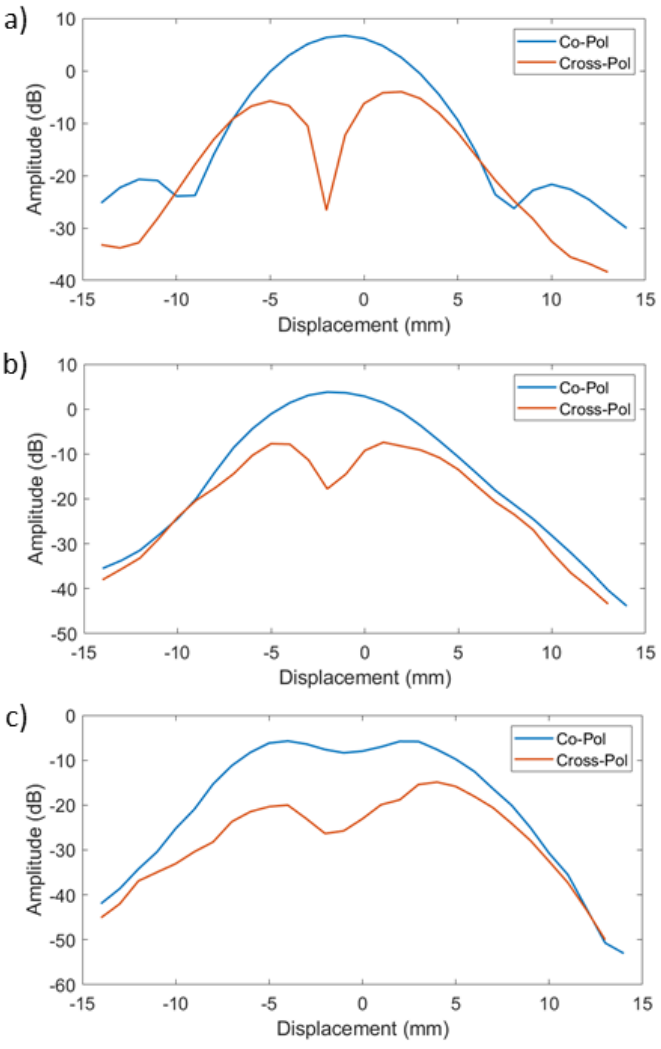

Fig. 4. Beam profiles along the x axis, for 0.25 THz, 0.5 THz and 0.85 THz.

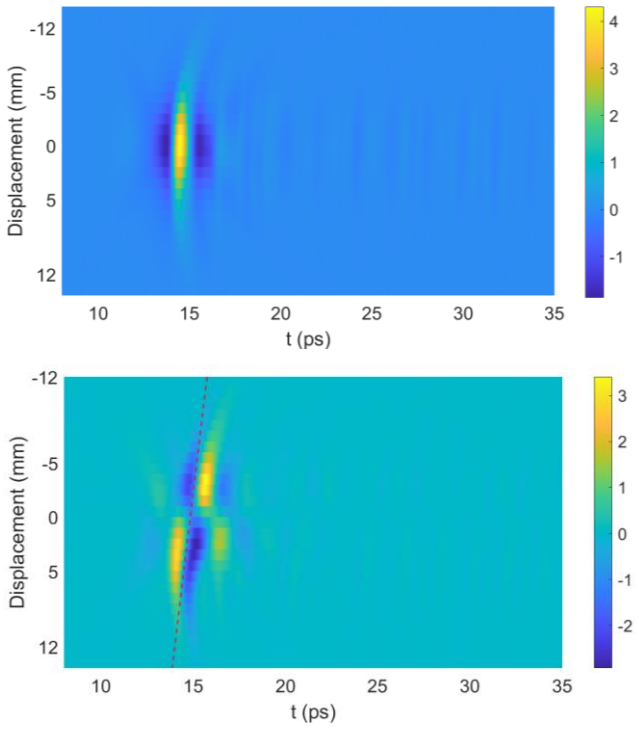

Fig. 5. Color scale images of the temporal waveforms as a function of x position of the aperture in the transverse plane with $y=0$, for the two polarization components. a) co-polar, and b) cross-polar. The dashed red line in b) highlights the detected tilt delay. Color palette in arbitrary units.

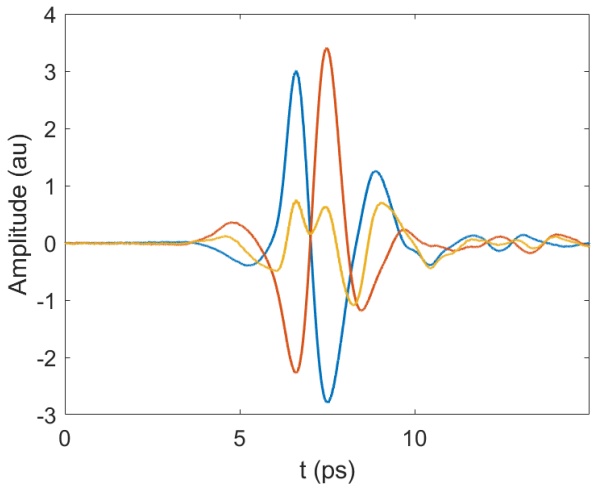

Fig. 6. Temporal waveforms in the cross-polar component at $x = -5\ mm$ (blue) and at $x = +5\ mm$ (orange) with 0.7 ps delay correction. The sum of both signals is shown in yellow.

Inspection of the temporal waveforms measured at the position of the maxima in the cross-polar component, with the $\Delta\theta\sim 0.6^0$ tilt correction, in Figure 6, reveals perfect pulse synchronization and a phase offset of approximately π radians, a characteristic feature of both Bow-tie and H-dipole patterns as seen in [15, 16].

It is instructive to closely analyze the relative values of both polarization components and the temporal evolution of the overall field polarization at the points of maximum cross-polar component. Figure 7 is a 3D plot where the vertical and horizontal axes correspond respectively to the temporal evolution of co-polar and cross-polar polarization components. By connecting the points in the 3D grid, a 3D trajectory is traced showing the temporal evolution of the tip

of the wave polarization vector in a transverse plane [17]. The projection over the z plane reveals a remarkable single-cycle circle signature with opposite handedness at each side of the LOS direction.

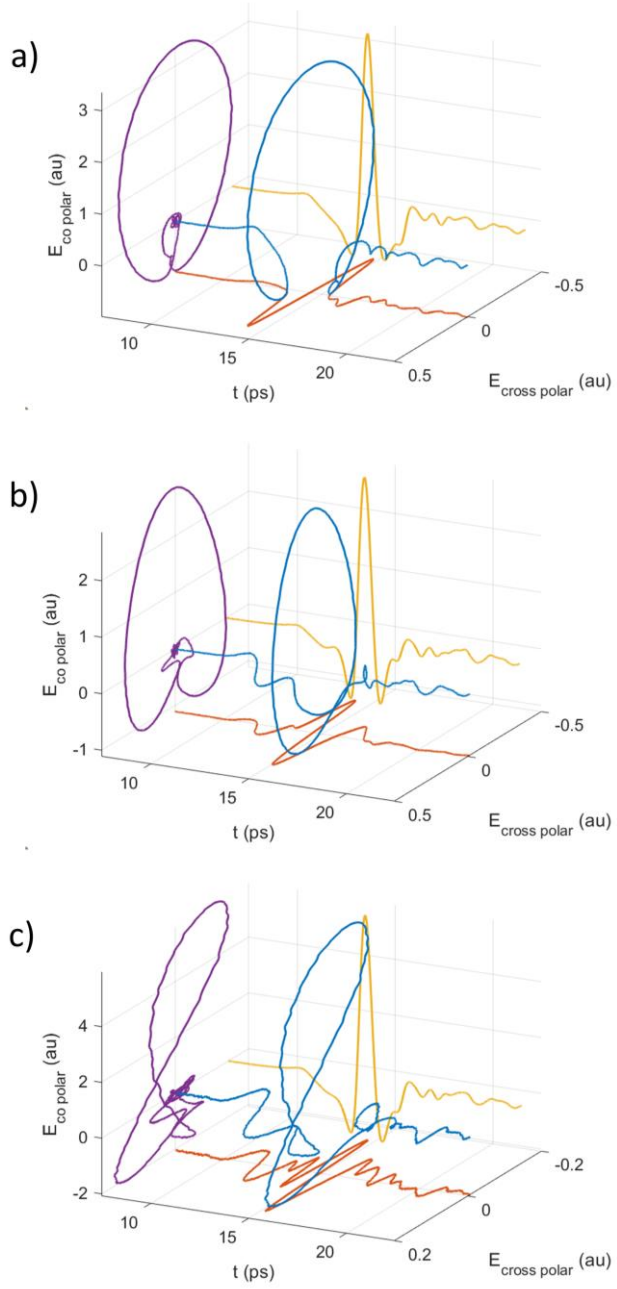

Fig. 7. Temporal waveforms at $x = -5\ mm$ (a), at $x = +5\ mm$ (b), with $\delta\tau = 0.07\ ps$ delay correction, and sum of both (c)

It is also significative to see how the addition of these two isolated waves yields an almost linear polarization in Figure 7 c). Monitoring the state of polarization at the LOS direction after a blocking plane with two holes at symmetric positions against LOS may thus constitute an appropriate technique to assess the correct alignment of a THz measurement setup.

IV. Conclusions

Measurements for the characterization of the spatial beam, polarization and propagation features of a system working at THz frequencies, and composed of a Bowtie TX and H-dipole RX, have been presented. The setup is simple and allows the use of fixed position antennas, compatible with free-space laser PCA alignment. Automated complete beam spatial and polarization characterization, and especially measurement of the cross-polar component, has been validated as a tool for detecting and correcting flaws in the measurement settings and for improving the systems performance in time domain THz spectrometers. Our results help to better understand the special features of THz radiation and pave the way towards simplified THz measurement setups, with special interest for the comparative analysis of THz devices and components.

Acknowledgements

This work was partly funded by the Ministerio de Economía y Competitividad under projects TEC2016-78028-C3-1-P, PID 2019-107885GB-C31 and MDM2016-0600, and Catalan Research Group 2017 SGR 219.

References

[1] S. S. Dhillon, *et al.*, 'The 2017 Terahertz Science and Technology Roadmap,' *J. Phys. D: Appl. Phys*., vol. 50, no. 4, 2017..

[2] F. Ellrich, M. Bauer, N. Schreiner, *et al.,* "Terahertz Quality Inspection for Automotive and Aviation Industries," *J Infrared Milli Terahz Waves*, vol. 41, pp. 470–489, Ap. 2020.

[3] I. Catapano, G. Ludeno, C. Cucci, *et al.*, "Noninvasive Analytical and Diagnostic Technologies for Studying Early Renaissance Wall Paintings," *Surv Geophys* , vol. 41, pp. 669–693, May 2020.

[4] D. Alves-Lima, J. Song, X. Li, A. Portieri, Y. Shen, J. A. Zeitler, H. Lin, "Review of Terahertz Pulsed Imaging for Pharmaceutical Film Coating Analysis," *Sensors*, vol. 20, no. 5, pp. 1441-1457, March 2020.

[5] R. Li, C. Li, H. Li, S. Wu and G. Fang, "Study of Automatic Detection of Concealed Targets in Passive Terahertz Images for Intelligent Security Screening," in *IEEE Transactions on Terahertz Science and Technology*, vol. 9, no. 2, pp. 165-176, March 2019,

[6] J.-H. Son, S. J. Oh and H. Cheon, "Potential clinical application of terahertz radiation," *Journal of Applied Physics*, vol. 125, 19090, 2019.

[7] H. Elayan *et al.*, "Terahertz Band: The Last Piece of RF Spectrum Puzzle for Communication Systems," *IEEE Open Journal of the Communications Society*, vol. 1, pp. 1-32, 2019.

[8] J. F. Molloy, M. Naftaly and R. A. Dudley, "Characterization of Terahertz Beam Profile and Propagation," in *IEEE Journal of Selected Topics in Quantum Electronics*, vol. 19, no. 1, pp. 8401508-8401508, Jan.-Feb. 2013.

[9] K. Elmabruk, K. Demir, H. Altan, *et al.*, "Time-Domain Characterization of the Radiation Pattern of the Terahertz Photoconductive Antennas," *J. Infrared Milli Terahz Waves*, vol. 40, pp. 595–605, 2019.

[10] P. U. Jepsen, R. H. Jacobsen, And S. R. Keiding, "Generation and detection of terahertz pulses from biased semiconductor antennas," *Journal of the Optical Society of America B-optical Physics*, vol. 13, no 11, pp. 2424-2436, 1996.

[11] P. Uhd Jepsen and S. R. Keiding, "Radiation patterns from lens-coupled terahertz antennas," *Opt. Lett.* , vol. 20, no. 8, pp. 807-809, 1995.

[12] G.Guimaraes and P. Reynaert, "Analysis of Substrate Mounted Dielectric Lenses for Silicon-based THz Sources," *2019 12th Global Symposium on Millimeter Waves (GSMM)*, Sendai, Japan, pp. 78-80, 2019.

[13] M. T. Reiten, S. A. Harmon, and R. Alan Cheville, "Terahertz beam propagation measured through three-dimensional amplitude profile determination," *J. Opt. Soc. Am. B,* vol. 20, no. 10, pp. 2215-2225, 2003.

[14] J. Van Rudd and Daniel M. Mittleman, "Influence of substrate-lens design in terahertz time-domain spectroscopy," *J. Opt. Soc. Am. B,* vol. 19, no. 2, pp. 319-329, 2002.

[15] J. Van Rudd, J. L. Johnson, and D. M. Mittleman, "Cross-polarized angular emission patterns from lens-coupled terahertz antennas," *J. Opt. Soc. Am. B* , vol. 18, pp. 1524-1533, 2001.

[16] J. V. Rudd, J. L. Johnson, and D. M. Mittleman, "Quadrupole radiation from terahertz dipole antennas," *Opt. Lett.* , vol. 25, pp. 1556-1558, 2000.

[17] E. Castro-Camus, "Polarization-Resolved Terahertz Time-Domain Spectroscopy," *J. Infrared Milli Terahz Waves,* vol. 33, pp. 418–430, 2012.

[18] S. Watanabe, "Terahertz Polarization Imaging and Its Applications". *Photonics* vol. 5, no. 58, 2018.

[19] J. Liu, W. Fan, B. Xue, "Dispersion control in fiber-coupled THz-TDS," *Optik*, vol. 123, no 24, pp. 2230-2232, 2012.

[20] E. Hecht, *Optics*. Reading, MA: Addison-Wesley, 2002, ch. 4.